ICCFD13 MILAN ITALY 2026
ICCFD13-2026-122

Cross-Verification of Fluid–Structure Interaction Frameworks for Supersonic Parachute Inflation

J. T. Durrant*, and F. Cadieux**
Corresponding author: tdurrant@stanford.edu
* Department of Aeronautics and Astronautics, Stanford University, CA, USA.
** NASA Ames Research Center, Moffett Field, CA, USA.

Abstract: In the past decade, the numerical simulation of supersonic parachute fluid–structure interaction (FSI) has advanced substantially through the development of Stanford's AERO Suite and, more recently, NASA's LAVA framework. Although both frameworks have been independently validated against data from the Advanced Supersonic Parachute Inflation Research Experiment (ASPIRE) flight tests, meaningful cross-verification of modern parachute FSI frameworks remains challenging due to the large number of interacting modeling choices present in the coupled problem. In this work, a systematic methodology for cross-verifying high-fidelity parachute FSI frameworks is developed and demonstrated using the ASPIRE SR03 test article. The proposed approach decomposes the coupled FSI problem into a hierarchy of structural, fluid, and coupled benchmarks, enabling sensitivities associated with individual modeling assumptions to be examined before considering the complete inflation process. Application of the methodology reveals close agreement in several isolated benchmark cases while also identifying sensitivities associated with structural discretization, fluid mesh representation, wall-boundary treatment, and porous-canopy modeling. Preliminary coupled simulations further demonstrate that modeling choices with modest influence in isolated analyses can become amplified in the fully coupled problem. These results establish a practical foundation for future code-to-code comparisons of parachute FSI simulations and highlight key challenges that must be addressed to achieve meaningful agreement between independent multiphysics frameworks.

Keywords: Fluid-Structure Interaction, Parachute, Supersonic.

1. Introduction

Parachutes remain the most reliable means of decelerating small payloads through the Martian atmosphere. They have been used successfully in every NASA Mars landing mission to date and will continue to play a central role in future robotic Mars missions. However, recent flight-test campaigns have experienced parachute failures [1, 2] whose underlying mechanisms remain poorly understood. Numerical simulations can provide detailed insights that are typically inaccessible in flight tests, such as local canopy stresses and individual line loads. Achieving such insight requires accurately capturing challenging physical phenomena, including shocks and turbulent wakes in the fluid, as well as fabric porosity and large nonlinear deformations in the structure. These challenges have driven the development of advanced frameworks for fluid–structure interaction (FSI) simulations of supersonic parachutes, including Stanford University's AERO Suite [3, 4, 5] and, more recently, NASA's Launch Ascent and Vehicle Aerodynamics (LAVA) framework [6, 7, 8].

Over the past decade, collaboration between Stanford University and NASA has driven significant advances in the simulation of supersonic parachute dynamics. The AERO Suite, developed by Stanford's Farhat Research Group, has progressively expanded its capabilities for coupled Eulerian computational fluid dynamics (CFD) and Lagrangian computational structural dynamics (CSD) [9, 10]. More recently, NASA's LAVA framework has been extended to support parachute FSI [7, 8]. Although LAVA FSI capability is newer and does not yet include some features available in the AERO Suite—such as data-driven anisotropic material laws [11] and two-way suspension-line coupling [12]—it provides an independent platform for high-fidelity parachute simulation and, therefore, a pathway to cross-verification.

Both frameworks have been validated independently against data from the Advanced Supersonic Parachute Inflation Research Experiment (ASPIRE) flight test campaigns [5, 8]. Code-to-code comparisons are routinely employed for NASA flight projects to increase confidence in numerical predictions and to quantify uncertainty associated with computational analyses. Extending such cross-verification efforts to complex multiphysics problems, however, introduces additional challenges. In fluid–structure interaction simulations, uncertainties arise not only from the fluid and structural discretizations individually, but also from the coupling strategies, interface treatments, and numerous modeling choices within each subsystem. While these differences may have modest effects in isolated analyses, they can become significantly amplified in the fully coupled problem. Furthermore, the use of immersed-boundary methods, adaptive mesh refinement (AMR), and highly deformable structures complicates traditional verification approaches such as systematic grid-convergence studies.

The objective of the present work is therefore not to establish complete agreement between two parachute FSI frameworks, but rather to develop and demonstrate a practical methodology for conducting such cross-verification studies. As illustrated in Figure 1, the proposed approach decomposes the coupled parachute FSI problem into a hierarchy of progressively coupled benchmark simulations, enabling fluid, structural, and coupling-related sensitivities to be examined independently before considering the fully coupled inflation problem. The resulting analysis provides an initial assessment of agreement between the AERO Suite and LAVA frameworks while identifying key sources of discrepancy and highlighting modeling sensitivities that warrant further investigation. In doing so, the study establishes a foundation for future code-to-code comparisons of high-fidelity parachute FSI simulations and demonstrates a systematic framework for tracing discrepancies in coupled predictions to their underlying modeling assumptions.

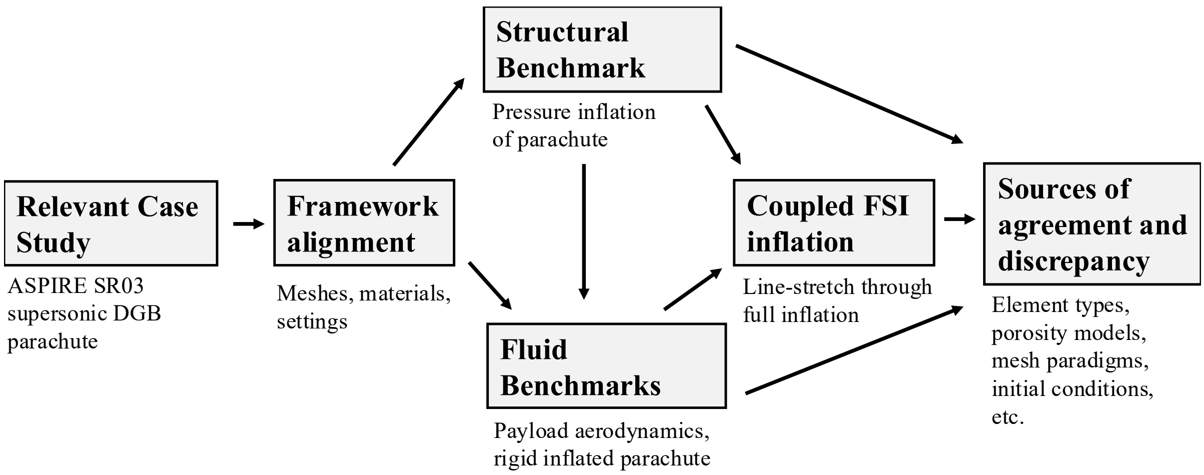

Figure 1: Progressively coupled cross-verification framework employed for the AERO Suite and LAVA FSI frameworks.

The remainder of this paper is organized as follows. Section 2 introduces the proposed cross-verification methodology, the ASPIRE SR03 test configuration, and the framework alignment process used to enable meaningful comparisons between the two simulation environments. Sections 3, 4, and 5 present the structural, fluid, and coupled fluid–structure interaction cross-verification studies, respectively, progressing from isolated benchmark problems to initial sensitivities and challenges faced in fully coupled parachute inflation simulations. Finally, Section 6 summarizes the principal findings, discusses the sources of differences identified throughout the study, and outlines directions for future cross-verification efforts.

2. Cross-Verification Methodology

This section describes the cross-verification methodology developed for high-fidelity parachute FSI simulations and its application to the AERO Suite and LAVA frameworks using the ASPIRE SR03 test configuration. Prior to comparison, key modeling assumptions are aligned between the two frameworks where possible to enable meaningful assessment of the remaining differences. The cross-verification process begins with isolated structural and fluid benchmarks before progressing to fully coupled FSI simulations, allowing sensitivities associated with individual modeling choices to be examined independently. For this initial study, the analysis focuses primarily on integrated quantities of interest, such as aerodynamic drag and canopy projected area, together with overall solution behavior, as these provide robust indicators of consistency between frameworks while establishing a foundation for future comparisons of more detailed local quantities.

2.1 ASPIRE SR03 Test Configuration

The ASPIRE SR03 flight test [13, 14] was selected as the reference case for the present cross-verification study. Conducted on September 7, 2018, SR03 was the third and final flight test of the ASPIRE program, which was developed to qualify the parachute system used for the Mars 2020 mission. During the test, the parachute deployed at an altitude of approximately 37.7 km and a freestream Mach number of 1.88, providing a well-documented supersonic inflation case for computational analysis.

The SR03 test article employed a Disk-Gap-Band (DGB) parachute [15], a configuration with extensive flight heritage that has been used in every successful NASA Mars landing mission since the Viking program. A schematic of the SR03 parachute system is shown in Figure 2, while the principal geometric parameters and deployment conditions are summarized in Table 1. The parachute system consists of a slender payload, a bridle and riser assembly, and the DGB canopy composed of a disk, gap, and band region.

The geometry and freestream conditions reported in Table 1 serve as the common reference configuration for all structural, fluid, and coupled FSI simulations considered in this study.

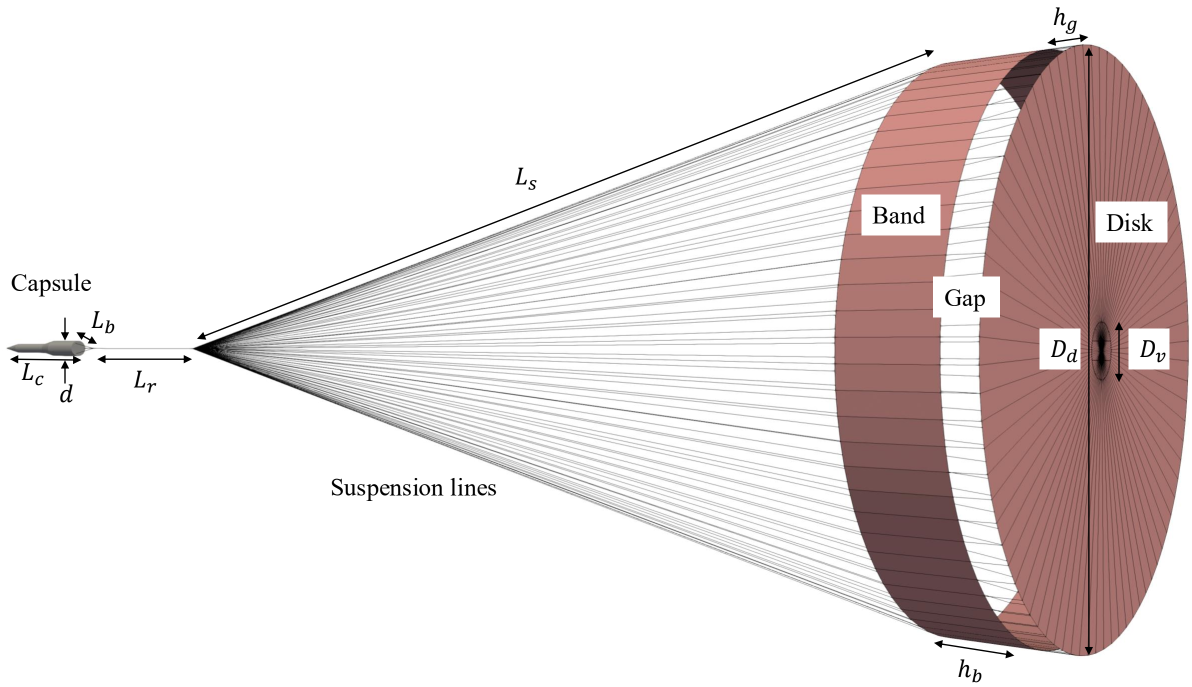

Figure 2: The ASPIRE SR03 Disk-Gap-Band (DGB) parachute system with geometric parameters labeled.

Table 1: ASPIRE SR03 flight test parachute geometry and freestream conditions at deployment.

Parameter	Symbol / Units	Value
Payload length	L_c [m]	6.67
Payload diameter	d [m]	0.72
Bridle length	L_b [m]	1.30
Riser line length	L_r [m]	7.7851
Disk diameter	D_d [m]	15.652
Vent hole diameter	D_v [m]	1.505
Gap height	h_g [m]	0.903
Band height	h_b [m]	2.6015
Deployment altitude	h_{deploy} [km]	37.7
Freestream Mach number	M_∞ [–]	1.88
Freestream velocity	V [m/s]	585
Angle of attack	α [°]	0.9
Freestream pressure	P_∞ [Pa]	414
Freestream density	ρ_∞ [kg/m^3]	6.01×10^{-3}
Reynolds number (based on D_d)	$Re_{D,\infty}$ [–]	3.3×10^6

2.2 Framework Alignment

Detailed descriptions of the relevant structural, fluid, and coupled FSI modeling approaches are provided in Sections 3, 4, and 5, respectively. Additional information on the two frameworks and their previous validation against ASPIRE flight-test data can be found in Refs. [5, 8]. The objective of the present work, however, is not to reproduce the previously published configurations exactly, but rather to align the two frameworks as closely as possible in order to isolate the impact of the modeling choices that remain distinct.

On the structural side, both frameworks employ geometrically nonlinear finite-element formulations capable of capturing the large deformations characteristic of parachute inflation. AERO Suite's structural solver, AERO-S, represents the canopy with membrane elements and supports advanced orthotropic and data-driven material models, while the LAVA structural solver employs MITC3 shell elements. For the present study, both frameworks are supplied with the same finite-element (FE) mesh consisting of 2.5×10^5 three-node canopy elements and 8×10^4 two-node elements for the suspension line system. The use of a common FE mesh eliminates geometric discrepancies from the comparison. To further improve consistency, the canopy material model is aligned by employing an isotropic Saint Venant–Kirchhoff hyperelastic law in both solvers, foregoing the orthotropic material laws typically applied in AERO for the woven parachute fabric. The suspension lines are likewise represented using comparable nonlinear bar elements in both frameworks. After alignment, the most important difference is in the canopy discretization: AERO Suite represents the canopy using membrane elements with no out-of-plane bending stiffness, whereas LAVA employs shell elements with finite bending stiffness.

On the fluid side, both frameworks are aligned to solve the compressible Navier–Stokes equations and employ immersed-boundary approaches to represent the parachute system without requiring a body-fitted mesh. AERO Suite's flow solver, AERO-F, employs a finite-volume discretization on an unstructured tetrahedral mesh with isotropic AMR. LAVA employs a Cartesian immersed-boundary formulation on a block-structured mesh with octree-based AMR and ghost-cell immersed-boundary techniques. The AMR criteria were also selected to provide comparable refinement of shocks and wake structures. In AERO Suite, refinement is driven by a Hessian-based indicator derived from the velocity field. An identical indicator was not available in LAVA, and therefore a temperature-based refinement criterion was employed instead. The LAVA indicator is based on a normalized measure of local temperature curvature and was selected because it produced refinement patterns qualitatively similar to those obtained with the AERO Suite velocity-based criterion. Although the refinement indicators are not identical, both frameworks concentrate resolution in regions containing shocks, shear layers, and wake structures. These differing mesh paradigms represent one of the most fundamental distinctions between the two frameworks and are therefore a primary focus of the present cross-verification.

Table 2: Key modeling choices in the cross-verification study. Bolded rows indicate the primary sources of discrepancy investigated in this work.

Modeling Choice	**AERO Suite**	**LAVA**
Structural discretization	Common mesh	Common mesh
Canopy material law	St. Venant–Kirchhoff	St. Venant–Kirchhoff
Suspension line model	Nonlinear bar	Nonlinear bar
Canopy element type	**Membrane**	**MITC3 Shell**
Fluid mesh	**Unstructured tetrahedral**	**Cartesian AMR**
Finest cell size	0.0064 m	0.0128 m
AMR indicator	Velocity Hessian	Temperature curvature
Suspension-line CFD model	Omitted	Omitted
Porosity model	**Flux–body force**	**Darcy–Forchheimer**
Wall boundary condition	**No slip**	**Slip**
Wall Function	Reichardt	Blended logarithmic
Flux function	HLLC	HLLEC
Limiter	Venkatakrishnan	Minmod
Time integration	Implicit DIRK2	Explicit SSPRK
Flow initialization	Payload wake preconditioning	Payload wake preconditioning
FSI coupling strategy	Partitioned	Partitioned
Initial parachute shape	Accordion fold	Gravity fold
Fluid–structure interface	FIVER	Ghost-cell method

To maintain consistency, comparable numerical schemes were selected where possible. AERO Suite employs the HLLC approximate Riemann solver with Venkatakrishnan limiting [16], while LAVA uses the closely related HLLEC flux function with Minmod limiting. Temporal integration also differs between the frameworks, with AERO Suite employing an implicit second-order DIRK scheme and LAVA employing an explicit strong-stability-preserving Runge–Kutta scheme. These choices may influence numerical dissipation and computational efficiency, but are generally considered secondary to the more fundamental differences in mesh paradigm, wall treatment, and porous-canopy modeling investigated in the present study. Additionally, both frameworks target comparable mesh resolutions and employ similar numerical settings where equivalent options exist. The suspension-line system is omitted from the flow solution in both frameworks to avoid introducing a modeling capability that is not available in both frameworks. Nevertheless, several important differences remain. The two frameworks employ different porous-wall models for the canopy: AERO Suite uses a homogenized flux–body force formulation for compressible porous flows [10], while LAVA employs a Darcy–Forchheimer model [7]. The solid wall treatments also differ between the two frameworks. AERO Suite employs no-slip wall boundary conditions together with a Reichardt wall function, whereas LAVA uses a slip-wall boundary condition (BC) with a blended logarithmic wall model. The slip-wall treatment is the recommended approach for wall-modeled LES in LAVA when the near-wall boundary layer is underresolved.

For the coupled inflation simulations, both frameworks adopt a partitioned FSI strategy where the fluid and structural subsystems operate on their own spatial and temporal discretizations. A similar initialization procedure is also adopted between the frameworks where a standalone CFD simulation of the payload is first performed to establish a realistic wake field before introducing the parachute system. However, differences remain in both the initial parachute shape and the fluid–structure coupling treatment. In AERO Suite, the canopy is initialized using an analytically prescribed accordion-folded shape, whereas LAVA employs a gravity-folding procedure that allows the canopy to collapse into a configuration with a small projected area relative to the oncoming flow. In addition, AERO Suite enforces the fluid–structure interface through the Finite Volume method with Exact Riemann (FIVER) approach [17], while LAVA employs a ghost-cell immersed boundary method.

The principal aligned and non-aligned modeling choices considered in the present cross-verification study are summarized in Table 2.

3. Structural Cross-Verification

To isolate structural differences between the two frameworks, a standalone pressure-inflation benchmark is considered prior to any fluid or coupled FSI simulations. The ASPIRE SR03 parachute is subjected to a prescribed uniform pressure of 1 kPa and integrated until a static equilibrium configuration is reached. Gravity is neglected and global damping is applied to remove excessive oscillations. The resulting canopy shape and projected area serve both as structural comparison metrics and as the reference geometry used in the subsequent rigid parachute aerodynamic simulations.

As discussed in Section 2.2, the structural models are closely aligned through the use of a common finite-element mesh, identical Saint Venant–Kirchhoff material properties, and comparable suspension-line representations. The primary remaining difference is the canopy discretization, with AERO Suite employing membrane elements and LAVA employing shell elements. Differences in contact treatment also remain, although contact effects are expected to play a larger role in the coupled inflation simulations considered later.

Figure 3 compares the equilibrium canopy geometries predicted by the two frameworks. Quantitatively, the projected canopy areas differ by approximately 1%, with LAVA predicting a slightly smaller inflated area than AERO Suite. This trend is consistent with the finite bending stiffness present in the shell formulation, which produces a modestly stiffer structural response than the membrane representation.

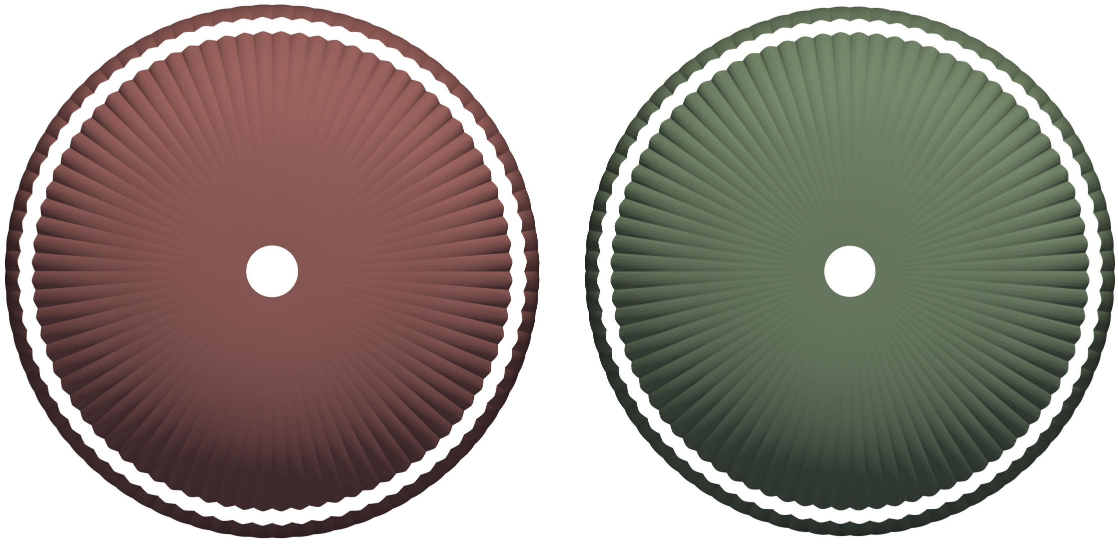

$A = 193.2\ m^2$ $A = 191.2\ m^2$

Figure 3: Inflated canopies and projected areas for AERO Suite (red, left) and LAVA (green, right) used for structural comparison and reference geometry in rigid parachute aerodynamic simulations.

More significantly, the close agreement demonstrates that the framework-alignment process successfully isolates the membrane-versus-shell distinction while removing most other sources of structural discrepancy. The resulting canopy shapes are nearly indistinguishable, and the projected areas differ by only approximately 1%. Since projected canopy area is one of the dominant geometric parameters governing parachute drag, this result provides confidence that subsequent differences observed in the rigid parachute aerodynamic simulations primarily arise from the fluid modeling rather than structural representation.

The resulting inflated geometries are therefore sufficiently similar to support meaningful aerodynamic comparisons in the following section.

4. Fluid Cross-Verification

Following the structural benchmark, a sequence of aerodynamic simulations is performed to investigate the fluid-modeling sensitivities identified in Section 2.2 before considering the fully coupled FSI problem. Particular emphasis is placed on integrated quantities of interest such as aerodynamic drag, as well as overall flow characteristics including wake structure and mesh adaptation behavior. These global metrics provide a robust basis for an initial cross-verification assessment. These global quantities are intentionally considered first, as meaningful comparison of more detailed local flow quantities requires establishing consistency in the dominant aerodynamic behavior of the two frameworks.

The primary fluid-modeling differences remaining after framework alignment are the mesh paradigm, wall-boundary treatment, and porous-canopy formulation. As discussed previously, AERO Suite employs an unstructured finite-volume discretization, while LAVA uses a Cartesian immersed-boundary approach with AMR. The two frameworks also employ distinct porous-wall formulations for the parachute canopy. The aerodynamic benchmarks considered in this section are designed to isolate the influence of these differences on both global quantities of interest and overall flow behavior.

Two aerodynamic benchmarks are considered. The first consists of a payload-only simulation that provides a baseline comparison of aerodynamic coefficients, wake structure, and mesh adaptation behavior. The second considers a rigid parachute aerodynamic benchmark using the inflated canopy geometry obtained from the structural benchmark. Additional variations of the rigid parachute case are used to separately assess the influence of wall-boundary treatment, payload-wake interactions, and canopy porosity on the resulting aerodynamic predictions.

4.1 Payload Aerodynamics

The ASPIRE flight-test payload consists of a slender payload with a diameter of 0.72 m at its largest end. Although the aerodynamic drag generated by the payload is small compared to that of the parachute, accurately capturing the payload flow field is important because the resulting turbulent wake strongly influences the downstream environment in which the parachute will inflate. In particular, interactions between the payload wake and the canopy bow shock have been shown to affect parachute inflation dynamics [18]. Consequently, the objective of this benchmark is not solely to compare payload drag coefficients, but also to assess the ability of each framework to resolve the wake structure that ultimately interacts with the parachute canopy. Drag coefficient therefore serves as a useful global quantity of interest, while wake characteristics and mesh adaptation patterns provide additional measures of consistency between the two fluid solvers.

The payload-only CFD simulations highlight the impact of the mesh paradigms employed by the two frameworks (unstructured in AERO Suite, Cartesian in LAVA). Figure 4 compares Mach contours and mesh overlays for the static payload configuration. The markedly different mesh paradigms and AMR strategies that track flow features are visible in the mesh overlays in Figure 4. Despite these differences, both frameworks initially predict payload time-averaged drag coefficients within approximately 1% of one another, as shown in Table 3.

As part of the framework-alignment process, additional studies were performed to assess the sensitivity of the payload aerodynamics to mesh resolution and wall-boundary treatment. Increasing the AERO Suite mesh from 7 to 37 million cells reduced the predicted drag coefficient from 0.34 to 0.31, indicating a non-negligible sensitivity of aerodynamic drag to mesh refinement, although both meshes were able to capture the turbulent wake moving downstream past the parachute location. Similarly, LAVA simulations were performed using both the recommended slip-wall treatment for under-resolved wall-modeled LES calculations and a no-slip wall boundary condition. The no-slip treatment reduced the predicted drag coefficient from 0.34 to 0.29. While these sensitivities influence the integrated aerodynamic coefficients, the primary objective of the payload benchmark is to establish a physically realistic turbulent wake for the downstream parachute simulations. To identify the converged drag value, a proper mesh convergence and sensitivity study without AMR would need to be undertaken. However, drag agreement alone is not sufficient to assess consistency between the frameworks; the resulting wake structure and its interaction with the parachute are of greater importance.

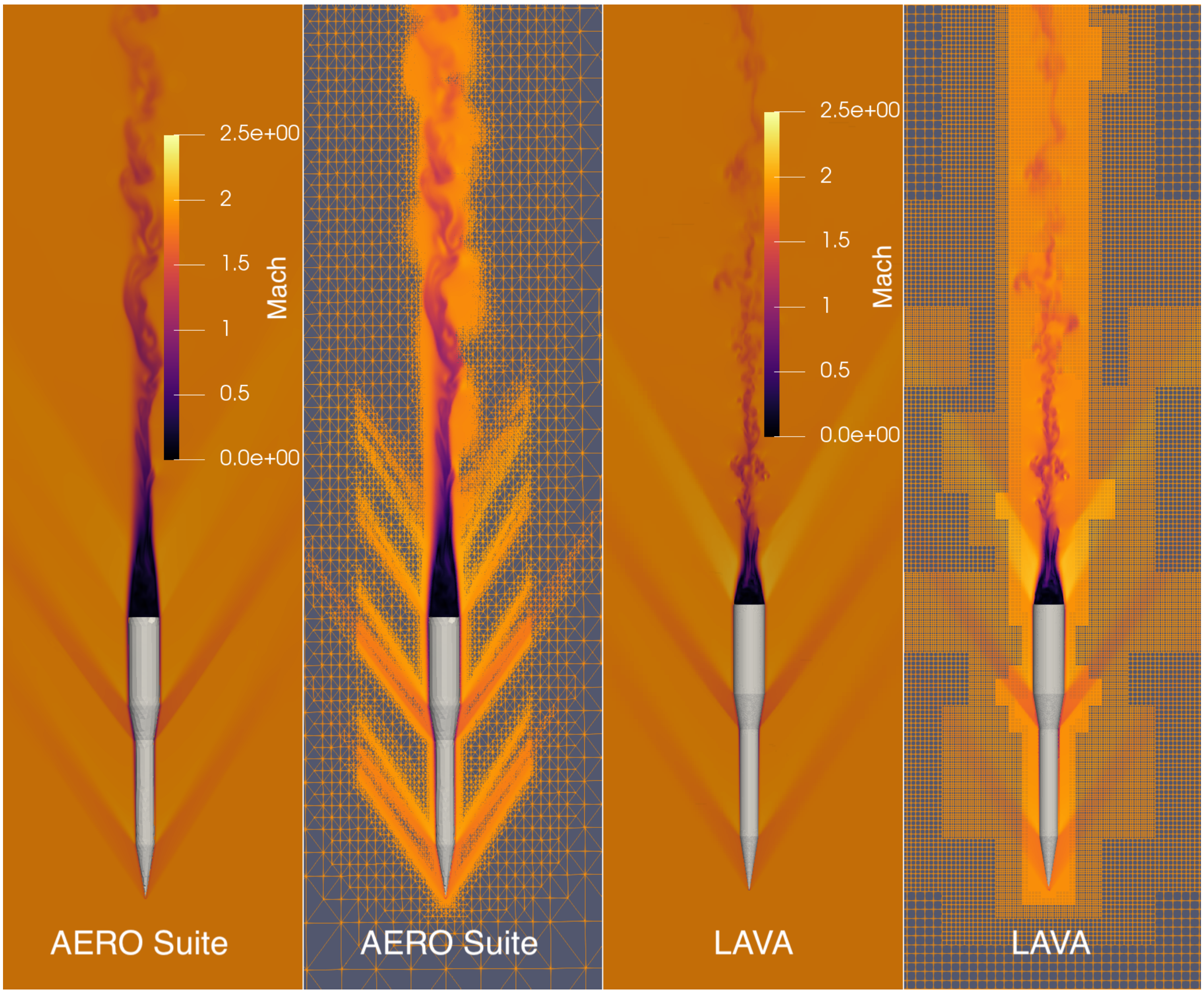

Figure 4: Mach contours and mesh overlays for the AERO Suite refined mesh (left) and LAVA slip BC (right) payload standalone CFD simulation.

Table 3: Payload CFD aerodynamic drag coefficients.

Framework	**Fluid Cell Count (million)**	C_D
AERO Suite	7	0.34
AERO Suite refined mesh	37	0.31
LAVA slip BC	25	0.34
LAVA no slip BC	20	0.29

The influence of the payload wake on parachute aerodynamics is examined more directly through the wake-deficit profiles shown in Figure 5. The figure compares the time-averaged normalized streamwise velocity at the parachute location for both frameworks along a line perpendicular to the freestream direction. To maintain consistency between the available datasets from the two frameworks, the profiles are averaged over only three solution snapshots and should therefore be interpreted as preliminary estimates of the mean wake structure rather than fully converged time averages. Despite differences in mesh paradigm, adaptive

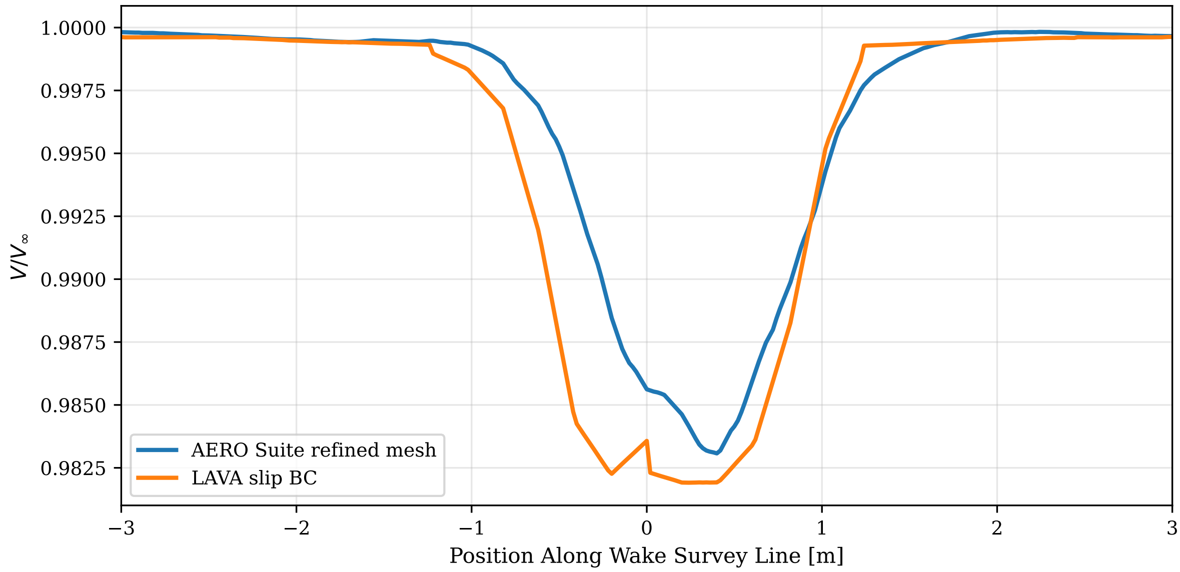

Figure 5: Comparison of normalized downstream velocities along a wake survey line perpendicular to the freestream flow at the parachute plane.

mesh refinement strategy, and wall-boundary treatment, both frameworks predict a similar wake-deficit profile at the parachute plane. The location and magnitude of the velocity deficit are captured consistently, suggesting that the large-scale wake structure ingested by the parachute is comparable between the two simulations. This agreement provides additional confidence that the aerodynamic environment encountered by the parachute during the subsequent rigid parachute aerodynamic benchmark is broadly consistent between the two frameworks.

4.2 Rigid Parachute Aerodynamics

The rigid parachute aerodynamic benchmark isolates differences in the fluid models while removing the complexities associated with structural deformation and fluid–structure coupling. In this case, the parachute geometry is fixed using the pressure-inflated canopy shape obtained from the structural benchmark described in Section 3. Consequently, any differences observed between the two frameworks arise from the fluid discretization, boundary-condition treatment, and porous-canopy modeling rather than structural response.

The drag coefficients reported in this section are computed using the projected canopy area predicted by each framework's structural inflation benchmark rather than a common reference area. Because the projected canopy areas differ by only approximately 1% (Section 3), the distinction is small for the present study. This choice avoids introducing an additional source of discrepancy through the drag-coefficient normalization and ensures that the reported differences primarily reflect variations in the aerodynamic predictions of the fluid solvers rather than differences in the selected reference area.

A particular focus of this benchmark is the treatment of canopy porosity. As described in Section 2.2, the two frameworks employ fundamentally different porous-wall formulations: AERO Suite uses a homogenized flux–body force approach developed for compressible porous flows while LAVA uses a Darcy–Forchheimer model. While both approaches are intended to represent the same physical phenomenon, their differing formulations may influence the resulting pressure distribution, wake structure, and aerodynamic loading.

To isolate the effects of the primary modeling differences, four rigid-body configurations are considered. These include the baseline payload-plus-parachute system with a porous canopy, the same configuration with a no-slip wall treatment in LAVA, a porous canopy without the payload, and an impermeable canopy

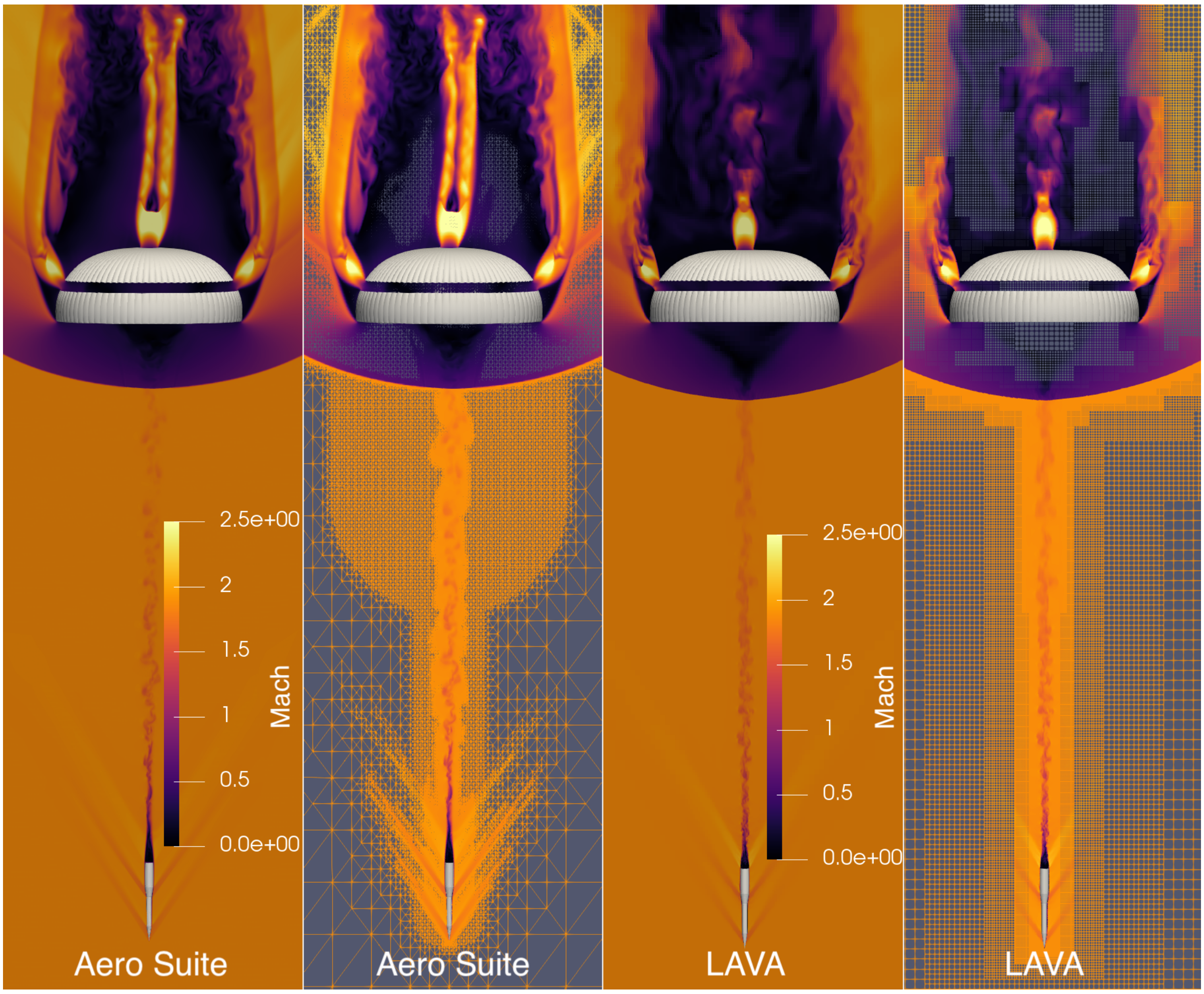

Figure 6: Mach contours and mesh overlays for the AERO Suite (left) and LAVA no slip (right) rigid payload + parachute CFD simulation.

Table 4: Rigid parachute aerodynamic drag comparison for the two frameworks for configurations with and without a payload and canopy porosity model.

Configuration	**AERO Suite C_D**	**LAVA C_D**	**% Difference**
Payload + Parachute (Porous)	1.38	1.47	6.5
Payload + Parachute (Porous, LAVA no slip BC)	-	1.43	-
Parachute Only (Porous)	1.44	1.54	6.9
Parachute Only (Impermeable)	1.49	1.57	5.4

without the payload. Together, these cases allow the influence of wall-boundary treatment, payload-wake interactions, and porous-canopy modeling to be assessed independently, while an additional grid convergence study would be necessary to compare converged drag values due to differing meshes between the two frameworks. Figure 6 compares Mach contours for the rigid parachute aerodynamic benchmark, while the corresponding time-averaged drag coefficients for all configurations are summarized in Table 4.

The first trend evident in Table 4 is the sensitivity of the predicted drag to wall-boundary treatment. Applying a no-slip boundary condition in LAVA reduces the drag coefficient from 1.47 to 1.43, bringing the prediction closer to the AERO Suite value of 1.38. However, this result should not be interpreted as evidence that the no-slip treatment is more accurate. Rather, it highlights the sensitivity of the solution to near-wall modeling assumptions in wall-modeled LES. Because the boundary layer is not fully resolved, the recommended slip-wall treatment in LAVA remains the preferred configuration despite the larger drag discrepancy.

The influence of the payload wake can be assessed by comparing the porous-canopy cases with and without the payload. Removing the payload increases the drag coefficient by approximately 0.06 in AERO Suite and 0.07 in LAVA, indicating that both frameworks predict a similar reduction in parachute drag due to wake ingestion. This agreement suggests that the overall impact of the payload wake is captured consistently despite differences in mesh paradigm and numerical implementation.

The final comparison isolates the influence of canopy porosity. As expected, making the canopy impermeable increases the drag coefficient in both frameworks because less flow is permitted to pass through the parachute. However, the magnitude of this increase differs noticeably between the two frameworks. AERO Suite predicts an increase in drag coefficient from 1.44 to 1.49 ($\Delta C_D = 0.05$), whereas LAVA predicts an increase from 1.54 to 1.57 ($\Delta C_D = 0.03$). Expressed in terms of the resulting aerodynamic force, this corresponds to a drag reduction of approximately 10 kN in AERO Suite and 7 kN in LAVA due to canopy porosity.

This result suggests that the homogenized flux–body force formulation and the Darcy–Forchheimer formulation produce different effective permeability characteristics despite being calibrated to represent the same canopy. While both frameworks predict the expected qualitative trend that canopy porosity reduces aerodynamic loading, the quantitative discrepancy indicates that porous-canopy modeling remains one of the most significant unresolved differences between the two frameworks. Given the central role of canopy porosity in supersonic parachute inflation, further investigation of both the prescribed porosity parameters and the underlying porous-wall formulations is warranted. Future work will employ identical inflated canopy geometries in both frameworks to eliminate geometric differences from the comparison and further isolate the sources of the remaining aerodynamic discrepancies.

Finally, although both frameworks employ adaptive mesh refinement, the distinct mesh paradigms lead to different distributions of resolution throughout the wake. In particular, neither configuration is expected to fully resolve all wake-recovery processes far downstream of the payload. Consequently, the present study focuses primarily on relative trends and integrated aerodynamic quantities rather than attempting to establish fully converged aerodynamic coefficients.

5. Preliminary FSI Sensitivities

The fully coupled FSI simulations represent the final and most sensitive stage of the cross-verification process. Unlike the isolated structural and fluid benchmarks considered previously, the coupled problem allows discrepancies in the fluid and structural representations to interact and compound through the fluid–structure coupling. As a result, even modeling choices that produce only modest differences in standalone CFD or CSD simulations may have a significant impact on the predicted inflation behavior.

Considerable effort was made to align the two frameworks prior to performing the coupled simulations. Both frameworks employ the same parachute geometry and structural mesh, identical freestream conditions, comparable fluid resolutions, and a similar initialization procedure. In each framework, a standalone payload CFD simulation is first performed to establish a realistic turbulent wake before introducing the parachute system in an approximated line-stretch configuration. The canopy is then released into this flow field and allowed to inflate under fully coupled fluid–structure interaction.

Initial efforts toward fully coupled FSI simulations using aligned AERO Suite and LAVA models have produced two important insights. First, the coupled inflation response is highly sensitive to combinations of modeling choices that appear relatively benign in isolated structural and fluid benchmarks. In particular, the interaction between the prescribed initial canopy shape and material model was found to strongly influence the early stages of inflation. AERO Suite typically initializes the canopy using an analytically prescribed accordion-folded configuration designed to represent a compact packed parachute state [5], whereas LAVA employs a gravity-folding procedure that allows the canopy to collapse into a streamlined configuration prior to deployment [8]. Initial observations from the coupled inflation simulations suggest that achieving meaningful code-to-code agreement will require careful consideration of the interaction between initial-condition generation and the aligned modeling assumptions adopted in each framework, which aligns with previous observations on the impact of initial conditions on certain parachute quantities of interest [19].

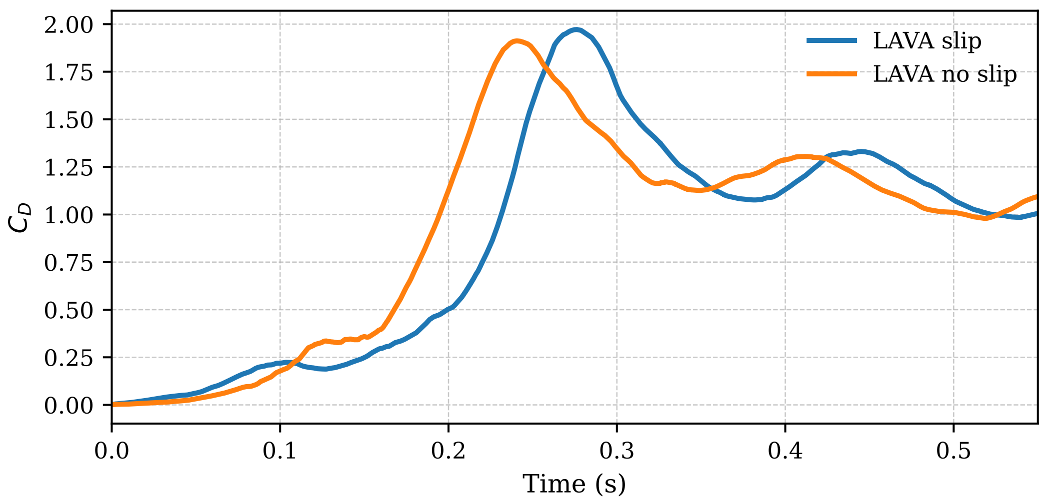

Figure 7: Drag time histories for the preliminary LAVA FSI sensitivity study, including slip and no slip BC treatment.

Table 5: LAVA FSI drag coefficient comparison for different wall BC treatments.

Configuration	**Peak C_D**	**Time to Peak (s)**
LAVA slip BC	1.97	0.276
LAVA no slip BC	1.91	0.241

The second key insight gained through the preliminary FSI simulations is the influence of wall-boundary treatment on the inflation dynamics. Figure 7 compares representative drag histories from an initial set of LAVA inflation simulations using the aligned modeling settings and inputs, while Table 5 summarizes the corresponding peak drag values and times to peak inflation load. Notably, the no-slip configuration reaches peak inflation approximately 13% sooner than the slip-wall configuration while simultaneously producing 3% lower peak drag. This trend differs from the expected inverse relationship between inflation time and peak load, where faster inflation is generally associated with larger peak drag [5].

Mach contours from representative time instances of the slip-wall and no-slip simulations are compared in Figure 8. Consistent with the differences observed in the drag histories, the two boundary-condition treatments produce noticeably different inflation trajectories and surrounding flow fields. At comparable stages of inflation, differences are visible in the canopy shape, flow structure through the gaps in the canopy and around the edges, and bow-shock position. In particular, the no-slip configuration pushes the bow shock away from the parachute system faster than the slip configuration.

These observations highlight a central challenge of FSI cross-verification: sensitivities that are small in isolated structural or fluid analyses may become amplified once the subsystems are coupled together. Consequently, meaningful code-to-code comparisons of parachute inflation dynamics require not only alignment of individual modeling assumptions, but also careful assessment of how those assumptions interact within the fully coupled problem.

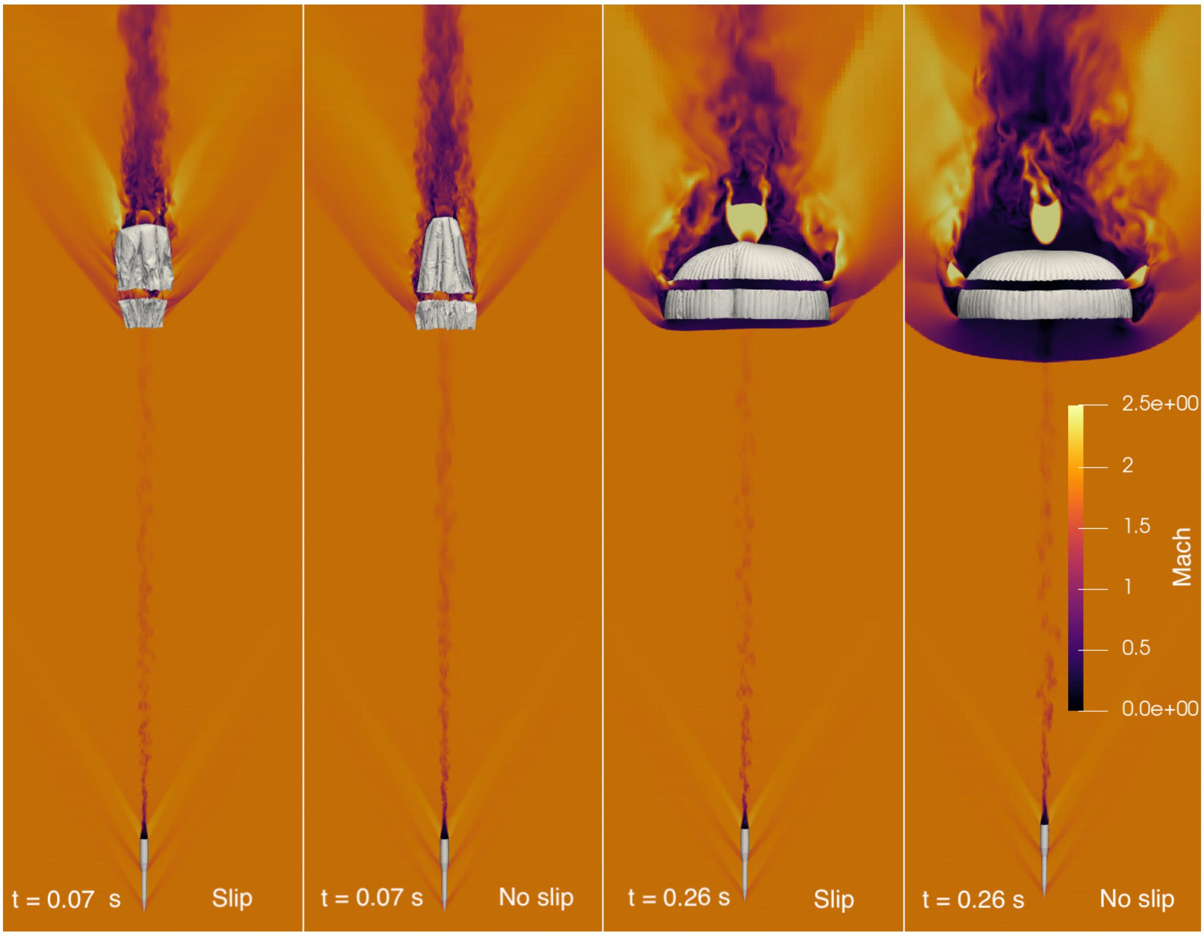

Figure 8: Mach contours from preliminary LAVA FSI simulations comparing slip-wall (left) and no-slip (right) boundary treatments at two representative stages of inflation.

6. Conclusion

Code-to-code comparisons are routinely employed for aerospace applications to increase confidence in numerical predictions and provide a measure of uncertainty in computational analyses. Extending these practices to complex fluid–structure interaction problems, however, presents additional challenges due to the large number of modeling choices, numerical discretizations, and coupling strategies that contribute to the final solution. This work presented and demonstrated a systematic methodology for cross-verifying high-fidelity frameworks for supersonic parachute fluid–structure interaction. Rather than comparing only fully coupled inflation simulations, the proposed approach decomposed the problem into a hierarchy of structural, fluid, and coupled benchmarks, enabling sources of agreement and discrepancy to be traced to specific modeling assumptions and implementation choices.

The structural cross-verification demonstrated close agreement between the two frameworks when a common finite-element mesh and material law were employed. The resulting inflated canopy geometries differed by approximately 1%, indicating that both frameworks predict similar global structural behavior despite differences in canopy element formulation. Because projected canopy area is a primary geometric driver of parachute drag, this result established a consistent structural basis for the subsequent aerodynamic comparisons.

The fluid cross-verification identified several important modeling sensitivities. Comparisons of the payload and rigid parachute aerodynamic benchmarks showed that mesh representation, wall-boundary treatment, payload-wake interactions, and porous-canopy modeling all influence the predicted aerodynamic loads. While both frameworks captured similar payload wake deficits and consistent qualitative trends in aerodynamic drag, differences remained in the predicted drag coefficients and in the effective reduction in drag associated with canopy porosity. These highlighted differences in the aerodynamic response associated with the porous-canopy models employed by AERO Suite and LAVA, while revealing residual drag discrepancies that persisted even in impermeable-canopy configurations.

The coupled FSI simulations revealed an even greater sensitivity to modeling assumptions than the isolated structural and fluid benchmarks. Modifications introduced to improve consistency between the two frameworks were found to influence the inflation response itself, demonstrating that modeling choices such as canopy material laws, initial canopy configurations, and wall-boundary treatments can become significantly amplified once the fluid and structural subsystems are coupled together. This observation highlights the utility of a staged cross-verification methodology, where sensitivities can be identified and investigated in isolated benchmarks before attempting direct comparisons of the fully coupled inflation dynamics.

Taken together, these results establish an initial framework for cross-verification of high-fidelity parachute FSI simulations while identifying several key sensitivities that warrant further investigation. Future work will focus on improving the fidelity of the aligned coupled configurations, extending the present methodology to additional quantities of interest, and isolating the root cause of the remaining discrepancies in aerodynamic drag. The ultimate goal is not only a rigorous code-to-code comparison of supersonic parachute inflation dynamics, but also the establishment of a practical methodology for cross-verifying complex multiphysics simulations relevant to future parachute systems.

Acknowledgements

This work was supported by the National Aeronautics and Space Administration through the NSTGRO program under award number 80NSSC24K1337. The authors would also like to acknowledge Faisal As'ad and Jason Rabinovitch for their contributions and help with this work.

References

[1] Clara O'Farrell, Erich J Brandeau, Christopher Tanner, John C Gallon, Suman Muppidi, and Ian G Clark. Reconstructed parachute system performance during the second ldsd supersonic flight dynamics test. In *AIAA Atmospheric Flight Mechanics Conference*, page 3242, 2016.

[2] Ian G Clark, John C Gallon, and Allen Witkowski. Parachute decelerator system performance during the low density supersonic decelerator program's first supersonic flight dynamics test. In *23rd AIAA Aerodynamic Decelerator Systems Technology Conference*, page 2130, 2015.

[3] Charbel Farhat, Philippe Geuzaine, and Gregory Brown. Application of a three-field nonlinear fluid–structure formulation to the prediction of the aeroelastic parameters of an f-16 fighter. *Computers & Fluids*, 32(1):3–29, 2003.

[4] Armen Derkevorkian, Jason Rabinovitch, Lee D Peterson, Philip Avery, and Charbel Farhat. Evaluation of an advanced suite of numerical codes for structural simulation of parachute fabric. In *2018 AIAA Aerospace Sciences Meeting*, page 1541, 2018.

[5] Faisal As' ad, Philip Avery, Charbel Farhat, Jason Rabinovitch, Marcus Lobbia, and Navid Ataei. Sensitivity analysis and validation of a computational framework for supersonic parachute inflation dynamics. *AIAA Journal*, 63(5):1743–1763, 2025.

[6] Cetin C Kiris, Jeffrey A Housman, Michael F Barad, Christoph Brehm, Emre Sozer, and Shayan Moini-Yekta. Computational framework for launch, ascent, and vehicle aerodynamics (lava). *Aerospace Science and Technology*, 55:189–219, 2016.

[7] Jonathan Boustani, Francois Cadieux, Gaetan K Kenway, Michael F Barad, Cetin C Kiris, and Christoph Brehm. Fluid-structure interaction simulations of the aspire sr01 supersonic parachute flight test. *Aerospace Science and Technology*, 126:107596, 2022.

[8] Francois Cadieux and Michael F Barad. Wall-modeled large-eddy simulation of supersonic

parachute inflation. *Computers & Fluids*, page 106800, 2025.

[9] Daniel Z Huang, Philip Avery, Charbel Farhat, Jason Rabinovitch, Armen Derkevorkian, and Lee D Peterson. Modeling, simulation and validation of supersonic parachute inflation dynamics during mars landing. In *AIAA Scitech 2020 Forum*, page 0313, 2020.

[10] Daniel Z Huang, Man Long Wong, Sanjiva K Lele, and Charbel Farhat. Homogenized flux-body force treatment of compressible viscous porous wall boundary conditions. *AIAA Journal*, 59(6):2045–2059, 2021.

[11] Faisal As'ad and Charbel Farhat. A mechanics-informed deep learning framework for data-driven nonlinear viscoelasticity. *Computer Methods in Applied Mechanics and Engineering*, 417:116463, 2023.

[12] Daniel Z Huang, Philip Avery, and Charbel Farhat. An embedded boundary approach for resolving the contribution of cable subsystems to fully coupled fluid-structure interaction. *International Journal for Numerical Methods in Engineering*, 122(19):5409–5429, 2021.

[13] Clara O'Farrell, Bryan S Sonneveldt, Chris Karhgaard, Jake A Tynis, and Ian G Clark. Overview of the aspire project's supersonic flight tests of a strengthened dgb parachute. In *2019 IEEE aerospace conference*, pages 1–18. IEEE, 2019.

[14] Bryan S Sonneveldt, Ian G Clark, and Clara O'Farrell. Summary of the advanced supersonic parachute inflation research experiments (aspire) sounding rocket tests with a disk-gap-band parachute. In *AIAA Aviation 2019 Forum*, page 3482, 2019.

[15] Ian Clark and Christopher Tanner. A historical summary of the design, development, and analysis of the disk-gap-band parachute. In *2017 IEEE Aerospace Conference*, pages 1–17. IEEE, 2017.

[16] Venkat Venkatakrishnan. Convergence to steady state solutions of the euler equations on unstructured grids with limiters. *Journal of computational physics*, 118(1):120–130, 1995.

[17] Charbel Farhat, Jean-Frédéric Gerbeau, and Arthur Rallu. Fiver: A finite volume method based on exact two-phase riemann problems and sparse grids for multi-material flows with large density jumps. *Journal of Computational Physics*, 231(19):6360–6379, 2012.

[18] Zp Kou and HR Zhan. Effects of forebody on supersonic parachute aerodynamic performance. In *Journal of Physics: Conference Series*, volume 2228, page 012013. IOP Publishing, 2022.

[19] Jeffrey T Durrant, Alexandra Haraszti, and Charbel Farhat. A computational framework for origami-inspired folding in high-fidelity fluid–structure interaction simulations. In *28th AIAA Aerodynamic Decelerator Systems Technology Conference*, page 3849, 2026.